THE PENNSYLVANIA STATE UNIVERSITY
SCHREYER HONORS COLLEGE

DEPARTMENT OF BIOMEDICAL ENGINEERING

SURFACE CHARACTERISTICS OF IMPLANTABLE LONG-TERM USE FONTAN PUMP MATERIALS

CLARE MCHUGH
SPRING 2019

A thesis
submitted in partial fulfillment
of the requirements
for baccalaureate degrees
in Biomedical Engineering and Mechanical Engineering
with honors in Biomedical Engineering

Reviewed and approved* by the following:

Keefe B. Manning
Professor of Biomedical Engineering and Surgery
Thesis Supervisor

Justin L. Brown
Associate Professor of Biomedical Engineering
Honors Adviser

* Signatures are on file in the Schreyer Honors College.

ABSTRACT

Penn State Hershey Medical Center is developing a small implantable pump for long-term mechanical support of patients with a failing Fontan circulation. An increasing number of patients who undergo the Fontan operation are surviving to adulthood and require a device to provide sustained support. Many blood contacting components of this pump are manufactured from polyetheretherketone (PEEK), which has not been thoroughly characterized with regards to its biocompatibility. This study analyzes the surface characteristics of PEEK and compares them to previously characterized pediatric pump polyurethane materials to analyze their thrombosis potential. Prior to analyzing platelet adhesion, the material surfaces of PEEK and polyurethane are studied using optical profilometry and x-ray photoelectron spectroscopy. An established rotating disk system protocol is used to test the adhesion of bovine platelets to the material surfaces at varying shear rates. The samples are analyzed with scanning electron microscopy and confocal microscopy. The samples prepared for confocal microscopy are stained, and these immunofluorescently labeled samples are imaged with a 20x dry objective to quantify the number of adhered platelets at different radial positions on the sample. Using platelet counts obtained from the confocal microscopy, the overall platelet adhesion for each of the PEEK and polyurethane samples was determined by calculating an adhesion coefficient. Overall trends in adhesion coefficient behavior showed the values decreased at higher shear rates. Material characterization techniques revealed consistent trends in platelet behavior across the different material samples.

TABLE OF CONTENTS

LIST OF FIGURES

LIST OF TABLES

ACKNOWLEDGEMENTS

I would like to first and foremost thank my research advisor, Dr. Keefe Manning, for his support and guidance over the past two years. I truly appreciate all of his advice and mentorship as an honors advisor, professor, and research advisor. I would also like to thank Dr. Justin Brown and Dr. William Weiss for serving on my thesis committee.

I would have been lost within my protocol and numerous questions without the help of Dr. Bryan Good. Bryan played an instrumental role in guiding my first year of research, helping collect data, and fielding my questions day and night. Thank you also to Sailahari Ponnaluri for answering countless questions and always being an encouraging voice in the lab. A huge thank you to my fellow lab members—Ceci Richardsen, Katie Blankemeyer, and Cara Pearson—for all of the support, laughs, late nights in Hallowell and the HUB, and research assistance. I would also like to thank Nadine at the Penn State Dairy farm for being so willing to help me in a moment notice on many early mornings.

I would like to extend my gratitude to all the members of the Penn State Artificial Heart laboratory, the members of the Division of Artificial Organs at Hershey Medical Center, particularly thank Dr. Lichong Xu for his assistance with polyurethane preparation and confocal and SEM imaging, and my funding provided by the Department of Defense W81XWH-16–1-053. Finally, none of this would be possible without the support of my family and friends for their endless support over these past four years. I truly could not have accomplished half of what I did over the past four years without you all.

Chapter 1

Introduction

1.1 Clinical Population

Congenital Heart Defects

Congenital heart defects are the most common birth defect. This condition affects 1%, or approximately 40,000 births in the United States each year. Of those 40,000 cases, 25% are labeled as critical heart disease.[1] Critical congenital heart disease occurs as a result of heart abnormalities during early embryonic development. Such conditions affecting the heart prevent effective blood flow, which subsequently reduces the amount of oxygen within the blood. Critical congenital heart disease may involve defects within the structure of the heart itself, vessels leading to or from the heart, or a combination of the two types of defects. Heart defects classified as critical congenital heart disease include coarctation of the aorta, double-outlet right ventricle, D-transposition of the great arteries, Ebstein anomaly, hypoplastic left heart syndrome, interrupted aortic arch, pulmonary atresia with intact septum, single ventricle, total anomalous pulmonary venous connection, tetralogy of Fallot, tricuspid atresia, and truncus arteriosus.[2] Treatment for these congenital heart defects vary; however, infants with critical congenital heart disease generally need surgery or other procedures during their first year of life.[1]

The Fontan Procedure

Approximately 3% of congenital heart defects result in a single ventricle anatomy, which historically has very high infant mortality rates.[3] Over the past several decades, treatments have

improved the survival of patients with these complex congenital heart defects through palliative surgeries.[3] One of these procedures is referred to as the Fontan procedure. The Fontan procedure was originally presented by Dr. Francis Fontan who developed the operative treatment in 1968, as a surgical treatment for tricuspid atresia.[4] The Fontan procedure is an approach to treat several congenital heart defects: tricuspid atresia, pulmonary atresia with intact ventricular septum, hypoplastic left heart syndrome, and double-inlet ventricle. The Fontan procedure is a palliative operation that has allowed patients with the single ventricle anatomy to increasingly survive toward adulthood.[5] The 'Fontan circulation' is used to generate a single ventricular system by connecting the systemic venous flow directly to the pulmonary artery.[6]

A number of modifications have improved Fontan's original procedure and its effectiveness as a palliative support. The modern procedure creates a connection of the inferior vena cava (IVC) and superior vena cava (SVC) to the pulmonary artery. The Fontan operation is typically performed in three different stages which are depicted in Figure 1.1.

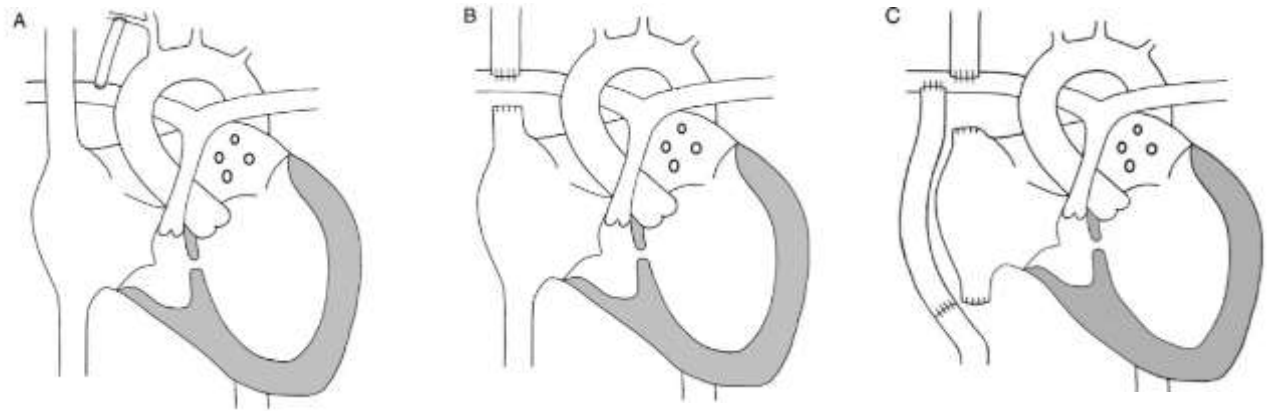

Figure 1.1 The three stages of Fontan procedure in tricuspid atresia. (A) First stage: artificial shunt placed between right subclavian artery and right pulmonary artery. (B) Second stage: anastomosis between right pulmonary artery and superior vena cava. (C) Third stage: completion of the Fontan circulation with extracardiac connection.[34]

The first stage is performed within the first few weeks of the neonate's life. This initial procedure places a systemic-pulmonary shunt in order to provide adequate pulmonary blood flow and relieve any existing systemic obstruction. The second stage occurs between four and twelve months and will include a superior cavopulmonary connection using either a hemi-Fontan or bidirectional Glenn technique. The third and final stage, the Fontan operation, completes the operation by connecting the IVC to the pulmonary artery via a conduit.[5] Two main methods exist for placing the conduit connection of the IVC and pulmonary artery—the extracardiac Fontan and the lateral tunnel Fontan. The conduit may be placed through the right atrial chamber (lateral tunnel Fontan), or it may run outside the heart to the right side of the atrium (extracardiac Fontan). Both of these anatomies are depicted in Figure 1.2.

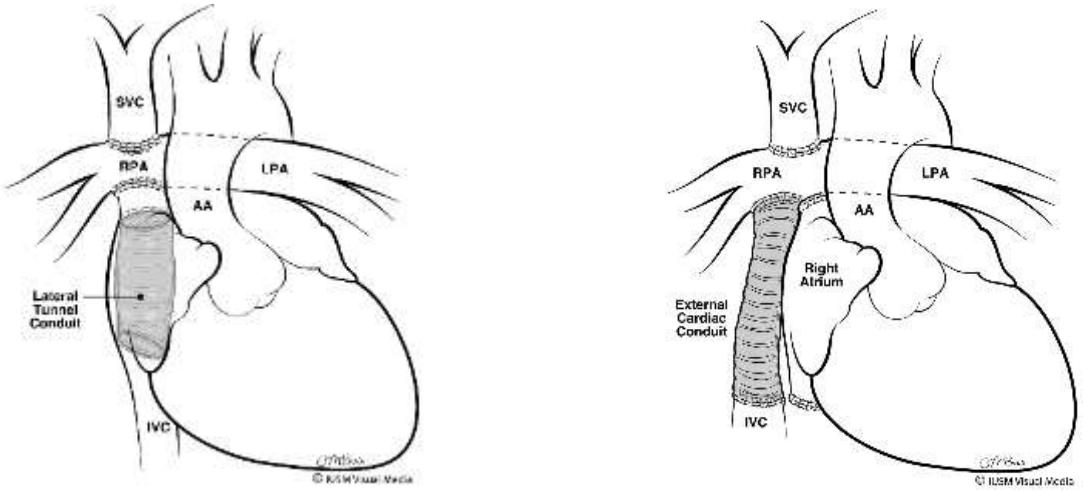

Figure 1.2 Diagram of the intraatrial lateral tunnel Fontan circulation (left) and the extraatrial conduit placement (right).[5]

As reported by the STS Congenital Heart Surgery Database, from January 2014 to December 2017, there were 3,379 Fontan operations.[7] This represents 2.8% of all congenital heart surgeries performed in the 119 reporting pediatric heart programs in the United States and Canada.[7]

Fontan Failure

The Fontan circulation allows for improved survival and better hemodynamic performance within single ventricle patients. With increasing survival rates of the surgical palliation in pediatric patients, a growing number of patients who undergo the Fontan operation suffer from unpredictable outcomes as an adult. Patients in this older population experience functional deterioration of the heart. This deterioration is marked by exercise intolerance and persistent cyanosis, arrhythmias, thromboembolism, plastic bronchitis, protein-losing enteropathy, and chronic right heart failure. This condition, associated with a number of different morbidities, is referred to as the "failing Fontan."[8] Figure 1.3 plots the cumulative death hazards posed over time following the Fontan operation. These patients who suffer from the failing Fontan are at increasing risk of death due to perioperative and other cardiac related risk factors. [9]

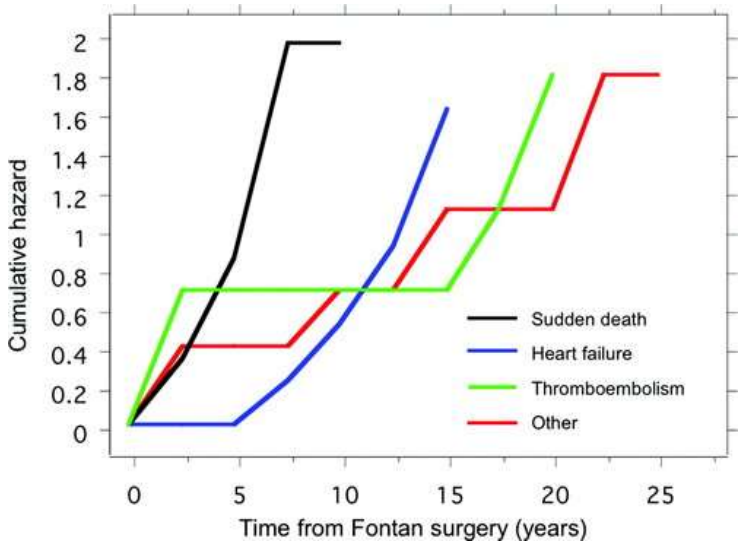

Figure 1.3 Plot of cumulative hazards (sudden death, heart failure, thromboembolism, other) vs. time from Fontan surgery.[9]

Patients within this Fontan failure population experience a state of chronic low cardiac output, and the single ventricular anatomy presents particular anatomical and physiological issues.

1.3 Fontan Failure Management

Current Treatment

Fontan completion has showed improved patient outcomes with low short-term operative mortality; however, long-term outcomes are poor.[46] The typical management of the failure state maintains the Fontan circulation with the intention of making patients better transplant candidates.[8] This is provided that patients are successfully bridged-to-transplant with mechanical circulatory support.[46] Heart failure vasodilators and pulmonary anti-hypertensive drugs are part of the clinical management of the Fontan failure.[8] These medical therapies are temporary solutions until a more permanent surgical solution is achieved.[8]

Mechanical circulatory support devices are also implemented in these Fontan failure cases to maintain the Fontan circulation. Extracorporeal membrane oxygenation (ECMO) is traditionally used for short-term mechanical support in pediatric heart failure. Ventricular assist devices (VADs) are increasingly being used with the Fontan circulation as a long-term bridge-to-transplant mechanism. Previous studies have explored the possibility of using these technologies as support for the failing Fontan. One study produced a computational and mock circulatory model of pediatric patients with diastolic, systolic, and combined diastolic and systolic Fontan failure.[10] This study evaluated the performance of VAD support, cavopulmonary assist device (CPAD) support, and combined VAD and CPAD support on the Fontan circulatory response.[10] The results of this study revealed that the Fontan circulation may be stabilized with cavopulmonary assist support during diastolic dysfunction, systemic VAD support during systolic dysfunction, and combined systemic and cavopulmonary support for combined systolic and diastolic dysfunction.[10] Berlin Heart EXCOR devices were tested with 26 patients with a functional single ventricle. The study

had a 42% success rate for bridge to cardiac transplant.[11] These rotary pumps designed as left ventricular devices are not optimized for the low head pressures within the Fontan circulation and the configuration of the pump is not designed for the Fontan anatomy.[39]

Efforts to create mechanical heart pumps for the Fontan circulation are in preliminary stages. Several technologies are in development for the cavopulmonary circulation; however, the optimal fluid dynamic conditions for the circulation under mechanical assistance is undetermined.[46] A continuous axial-flow pump developed by Wei *et al.* was tested in piglet models with a modified Fontan circulation. The study showed that the pump could provide temporary circulatory support for the Fontan circulation.[36] Dr. Amy Throckmorton has proposed a number of designs to operate within these unique anatomical conditions. Five distinctive two-bladed folding-blade propeller prototypes were designed and evaluated with computational fluid dynamics.[47] The results of these designs achieved a reduction of fluid stress levels, removal of recirculation regions, and improved hydraulic performance of the folding propeller.[47] The propeller design produced the physiological pressures and flows within the ideal range for mechanical support of the univentricular Fontan circulation.[47] Throckmorton also proposed a design of a protective cage for a collapsible, percutaneously inserted, axial pump.[48] The outer cage was designed with radially positioned filaments to protect the vessel wall from rotating pump components.[48] A numerical analysis of 13 models demonstrated acceptable hydraulic performance of the pump.[48] A collapsible, percutaneously-inserted, axial flow pump with a four-bladed impeller was evaluated with numerical, hydraulic, and hemolytic testing by Throckmorton *et al.*[49] The experimental and numerical predictions showed strong agreement with a maximum deviation of less than 6%.[49] Dr. Mark Rodefeld, in collaboration with the NASA Glenn Research center, is developing a small electric-driven bi-conical heart pump to maintain the Fontan circulation.[37] Using a three-bladed

folding-blade propeller pump design, Throckmorton and Rodefeld *et al.* have developed a prototype for the pump. The testing has shown to have pressure-flow characteristics and minimal hemolysis that make it an ideal temporary pump.[38]

Penn State Fontan Pump

Penn State Hershey Medical Center is creating a long-term mechanical pump with sustained support of the Fontan circulation. The proposed design is intended to provide long-term support specifically for the failing Fontan and serve as a bridge-to-transplant or destination therapy technology. This design is intended to configure to the total cavopulmonary connection and optimize the low head pressures within the pulmonary circulation. The blood contacting materials within the pump are commercially pure titanium and polyetheretherketone (PEEK). An implantable rotary blood pump has been created and evaluated by Cysyk *et al.*[39] A 30-day *in vivo* sheep study revelated successful implantation and postoperative recovery. The pump demonstrated adequate circulatory support and maintained normal physiologic pulmonary and venous pressures.[39]

1.5 Medical Device Biocompatibility

Biocompatibility may be defined as the "ability of a material to perform with an appropriate host response in a specific application."[12] Biomaterials play an essential role in the function and design of a medical device, as the tissue-material interaction may be indicative of the device's performance.[13] Various surface characteristics such as texture, smoothness, and roughness

contribute to the biological reaction of the material and must be accounted for within material selection.

Platelets and Fibrin

Platelets and fibrin are components of the blood that are involved in the blood-material interactions through the clotting process. Platelets, or thrombocytes, are small, discoid components of blood that are approximately 2-4 microns in diameter. These anuclear bodies depicted in the diagram in Figure 1.4 are created from the fragmentation of megakaryocytes in the bone marrow. Platelets, on average, have a lifespan of approximately 10 days, and the average human platelet count ranges between $150x10^6$ – 450x106.[16] Platelets have a key physiological role in hemostasis, a mechanism of the body that prevents blood loss when a wound causes disruption to the vasculature. Platelet activation may occur in response to exposed collagen from a wound, the presence of foreign materials, bulk phase agonist, or mechanical stresses.[16]

Figure 1.4 Micrograph of a round aggregation of platelets (1000x). [50]

Fibrin is an insoluble protein arranged in long fibrous chains and formed from fibrinogen (Figure 1.5).[51] Human plasma, on average, contains around 1.5 to 3.5 g/L of fibrinogen.[52]

Fibrinogen is converted to fibrin through thrombin-catalyzed cleavage of two fibrinopeptide pairs.[52] Fibrin is a viscoelastic polymer that possesses high extensibility and compressibility, which contributes to its ability to have high deformability without rupture.[52]

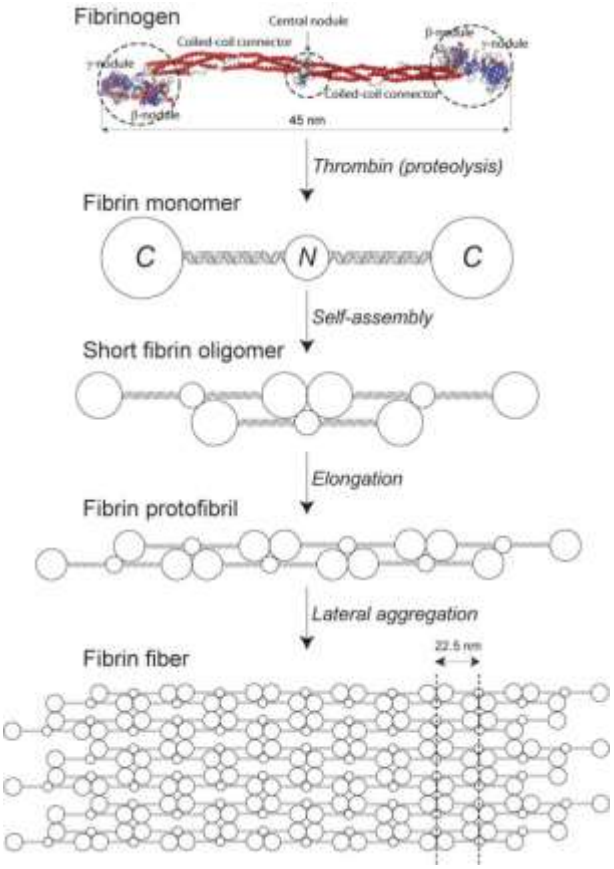

Figure 1.5 Schematic of fibrin polymerization.[51]

Hemocompatibility and Thrombosis Formation

Hemocompatibility is defined by the "blood material interactions with biomaterials that do not cause thrombosis, emboli, hemolysis, activation, or denaturation of plasma proteins."[12] A main consideration with biocompatibility is hemocompatibility, which is a great concern particularly for cardiovascular devices. These devices are directly in contact with blood and their function and response is dictated by this interaction. When a biomaterial contacts blood, proteins are adsorbed

to the surface, which acts as a primary event to initiate the coagulation pathway. This pathway is initiated through the adhesion and activation of platelets and the activation of proteins of the intrinsic coagulation cascade.[15] The coagulation pathway (Figure 1.6) is vital to the understanding of the interaction of biomaterials and occurrence of thromboembolism, which is a frequent complication and design consideration for cardiovascular medical devices.

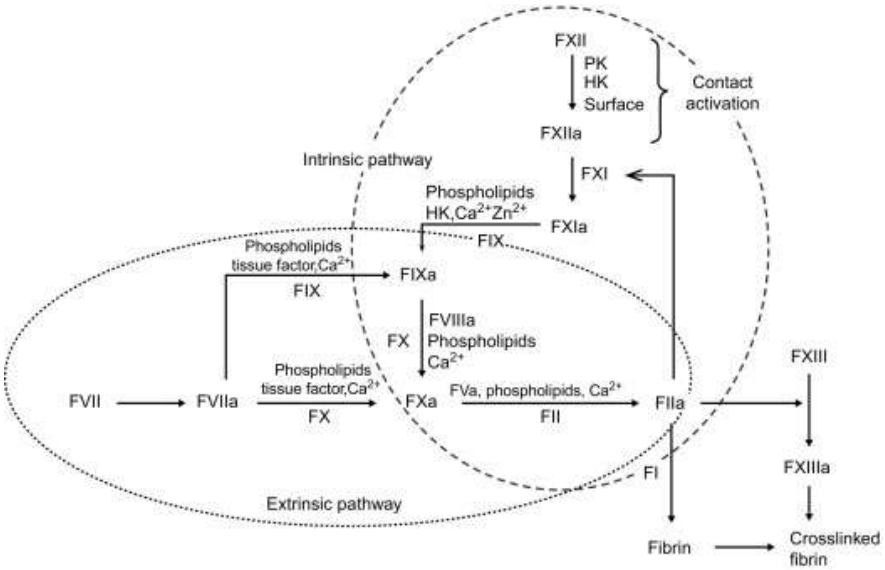

Figure 1.6 Simplified plasma coagulation cascade emphasizing the intersection of the intrinsic and extrinsic pathways. For simplicity, mediators, cofactors, inhibitors, and amplification loops are not shown.[15]

Shear stresses are a contributing factor to platelet activation. The highest shear stresses in the normal human circulation range from 500 to 5,000 s^{-1}.[17] Platelet activation and aggregation contribute to thrombus formation. Thrombus formation on devices occurs partially due to these platelet reactions of adhesion, activation, and aggregation and the coagulation of blood plasma. The development of thrombi on device surfaces is one of the main problems in long-term blood-contacting devices.[18]

Blood-material interactions also vary with the blood species; platelets have varied responses to materials.[19] Large ruminant platelets such as those of cattle, sheep, and goats have similar structure and function. Bovine platelets have been thoroughly studied regarding their structure, adhesion, and aggregation. Bovine platelets, similar to those of humans, are discoid in shape and 1-5 micrometers in diameter.[19] Ruminant platelets generally are less responsive to agonists compared to other species and adhere to subendothelial collagen less readily than platelets of other species.[19] Platelet responses to biomaterials vary as well. In a study by Goodman *et al.*, ovine platelets were found to be "considerable attenuated in their response to biomaterials compared to human platelets."[20] This reveals that, while sheep are appropriate in modeling some aspects of cardiovascular biocompatibility such as hemodynamics and calcification, sheep platelets do not attach, spread, and grow in the same manner as human platelets.[20] A study by Pelagalli *et al.* studied the platelet aggregation profile and marked differences in platelets from humans and four animal species to adhere to autologous immobilized fibrinogen. These results similarly showed that sheep platelets, compared to human platelets, attach to biomaterials less effectively and are less active overall.[35]

Polyurethane Urea (PUU) Biocompatibility

Polyurethane urea (PUU) has a history of medical applications and material properties that demonstrate biocompatibility. Polyurethanes have been used for medical devices since the late 1960s.[13] These block copolymers (Figure 1.7) typically have an ether or ester soft segment and an aromatic or aliphatic hard segment and urethane or urethane urea linkage. These applications include artificial hearts, intra-aortic balloons, pacemaker leads, heart valves, and

hemodialysis membranes. Polyurethanes have strong chemical and abrasion resistance, strength, and due to its manufacturability and versatility, a variable measure of durability, flexibility, and toughness. The formulation of polyurethanes vary and the formulation can contribute to the optimization of properties, particularly density.[56] Polyurethane also has a high degree of hemocompatibility, which contributes to its effectiveness in medical devices.[13]

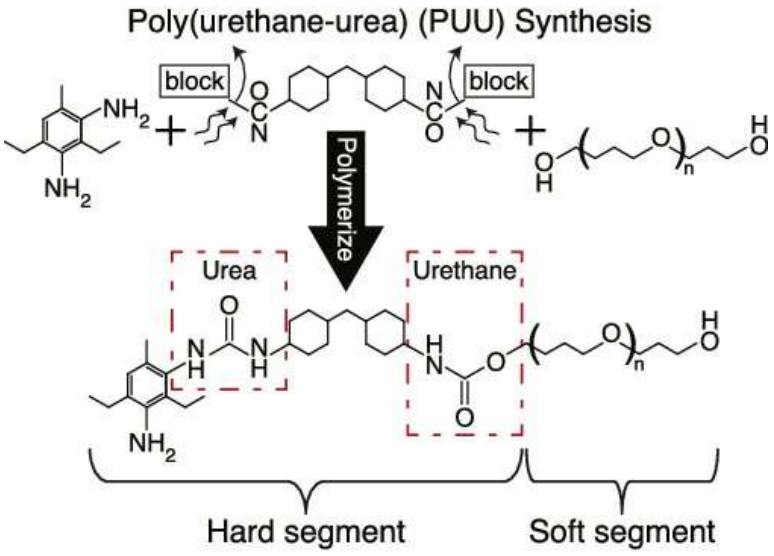

Figure 1.7 Polyurethane urea chemical structure and synthesis.[53]

Polyetheretherketone (PEEK) Biocompatibility

Polyetheretherketone (Figure 1.8) is a high-performance thermoplastic polymer that has been of interest to the medical community since the late 1980s for its versatility, compatibility with imaging techniques, and desirable mechanical properties such as a high strength, rigidity, and toughness.[12,14] PEEK also has excellent stability at high temperatures, resistance to chemical and radiation damage, a low coefficient of friction, low permeability, compatibility with many reinforcing agents, and greater strength (on a per mass basis) than many metals.[12,14] The

semicrystalline polymer has a density of 1.32 g/cm^3 and has high wear-resistance, fatigue and creep resistance, and resistance to hydrolysis.[55]

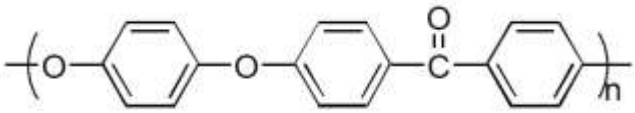

Figure 1.8 Polyetheretherketone (PEEK) repeat unit structure.[54]

1.6 Previous Studies

Platelet adhesion studies have been performed to evaluate platelet adhesion to biomaterial surfaces. Previous studies have evaluated the performance of polyurethane and extensive results exist that categorize its biocompatibility and hemocompatibility. A 1986 study investigated the visualization and analysis of thrombogenesis on collagen-coated glass, nylon, and polyurethane.[21] The study used a parallel plate flow chamber with steady flow whole blood at a constant shear rate of 100 s^{-1}, 500 s^{-1}, or 1000 s^{-1}. The polyurethane results revealed that at the lowest shear rate, 100 s^{-1}, many small to moderate thrombi adhered to the surface and rapidly embolized.[21] However, a few of the thrombi did not embolize and instead remained stable on the surface. At the higher shear rates, there were a number of temporary adhesive encounters of single platelets with the surface. Furthermore, few large emboli formed and no stable thrombi were identified on the surface. The study hypothesized that platelets are unable to form stable surface bonds at shear rates greater than 500 s^{-1}.[21] A 2002 study reported similar findings when examining the effects of co-adsorbed proteins and shear forces with polyethylene, polytetrafluoroethylene, and silicone rubber tested at shear rates of 0 s^{-1}, 200 s^{-1}, 500 s^{-1}, and 1000 s^{-1}.[22] All of the polymers showed minimal platelet adhesion at 1000 s^{-1}. Furthermore, the study indicated that fluid shear, residence time of the

adsorbed protein, nature of the co-adsorbed proteins, and surface chemistry of the material all play a role in influencing the platelet-surface interaction and biocompatibility.[22]

Rotating disk systems have been used to investigate adhesive properties of biomaterials, such as polyurethane materials. A rotating disk is ideal for analyzing biomaterials as it has a well understood flow field at the surface.[23] A linear relationship between shear rate and radial distance is used to investigate the effects of adsorbed platelets at varying radial distances and shear ranges when using a disk. These studies have quantified the effects of hematocrit on rotation time with PUU and the effects of pulsatility and quantified levels of shear. Another rotating disk study analyzed the effects of sub-micron PUU texturing on platelet adhesion.[24] The results revealed that sub-micron texturing may assist in reducing platelet adhesion in areas of low shear stress.[24] The rotating disk model was also used to investigate the effects of peak shear on platelet adhesion. Adhesion levels were found to depend on peak platelet flux and shear form, and platelet adhesion was found to decay exponentially with increasing shear rate.[25,45] Platelet adhesion to smooth PUU after two hours was greatest in the shear region of 0 s^{-1} to 333 s^{-1}, and high shear rates showed minimal platelet attachment.[25]

1.8 Present Study

The present study uses a rotating disk system (RDS) and imaging and surface categorization techniques (optical profilometry and x-ray photoelectron spectroscopy) to study a polyetheretherketone material. The results of the surface categorization and RDS will be primarily compared to polyurethane, which has been thoroughly studied regarding its biocompatibility within pediatric cardiovascular devices. The study will investigate the effects of bovine platelets

to predict the reaction of this material interaction with other animal species and human blood in the Penn State Fontan pump.

Chapter 2

Theory

2.1 Optical Profilometry

An optical profilometer is a white light interferometer that produces high precision 3D metrology of surface features. Optical profilometry is a rapid, nondestructive, and noncontact surface metrology technique.[41] The optical profiler uses coherence scanning interferometry to measure surface topography.[41] The measurement types include flatness, roughness, steps and segments, thin films, and steep slopes, with feature heights ranging from less than 1 nm to 20 mm.[41]

2.2 X-Ray Photoelectron Spectroscopy

The x-ray photoelectron spectroscopy technique is based on the Photoelectric Effect, which states that photoelectrons are ejected from atoms in the near surface when a material is irradiated with x-rays.[42] The signal detected originates from the outer 1-10 nm of the sample, and the spectra contains information about elemental composition, concentrations, and chemical environments of surface and near surface atoms.[42] The XPS technique has a number of capabilities including high surface sensibility; elemental analysis, in-depth compositional information via argon ion beam depth profiling; chemical state imaging with high lateral resolution; breath of sampling types such as thin-films, powders, fibers, and bulk materials; and sample cooling and heating.

2.3 Rotating Disk System

The flow field near the surface of a rotating disk has been thoroughly characterized.[30,31] Flow within the boundary layer of a rotating disk is determined by viscous stresses that cause the fluid to rotate. The shear stress in a thin layer of fluid at the boundary layer of the rotating disk surface is a linear function of the radial distance from the center. Shear stress was calculated at any location on the disk with Equation 1[33],

$$\tau = 0.80\eta r \left(\frac{\omega^3}{\upsilon}\right)^{0.5} \quad [1]$$

where τ is the shear stress magnitude at the surface (dynes/cm^2), η is the absolute viscosity of the medium (poise), r is the radial distance from the center of the disk (cm), ω is the angular velocity (radians/second), and υ is the kinematic viscosity (Stokes). This equation is based on the assumptions that the disk is infinitely large and rotating in an infinite medium, steady state conditions apply, and laminar flow exits in the boundary layer at the material surface.[33] Since the average platelet diameter is 2-4 μm, the relative dimensions of the rotating disk provided a valid approximation of the infinite disk and medium assumption.[33] The disk in the experiment is used with a steady angular rotation.[33] The selected dimensions and volumes in the experiment ensure that these theoretical constraints were met.[33]

2.4 Scanning Electron Microscopy

A scanning electron microscope (SEM) is a non-destructive technique that uses focused source of high energy electrons to scan a surface and create a high-resolution image. The accelerated electrons emitted by the SEM carry kinetic energy that is dissipated as signals when the incident electrons are decelerated in the electron-sample interactions.[57] The signals generated

at the interface of the sample and the electron beams also reveal surface information such as external morphology, chemical composition, and crystalline structure and orientation.[57] Conventional SEM techniques have magnification ranges from 20x to approximately 30,000x with spatial resolution of 50 nm to 100 nm.[57] Components of a scanning electron microscope are depicted in Figure 2.1.

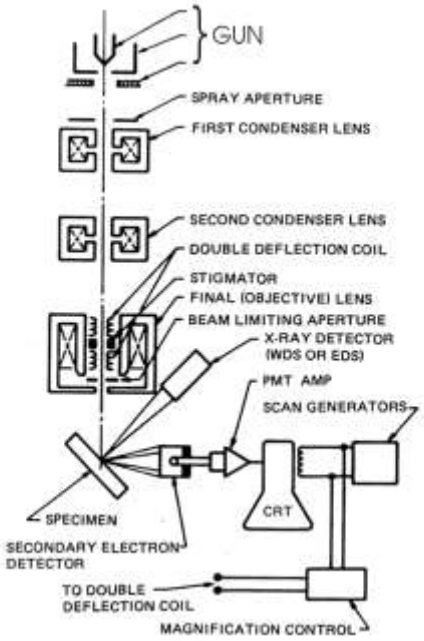

Figure 2.1 Scanning electron microscope schematic.[57]

2.5 Confocal Microscopy

The confocal fluorescence microscope consists of multiple laser excitation sources, a scan head with optical and electronic components, electronic detectors, and a computer for acquisition, processing, and analysis.[32] Light with a user-specified excitation wavelength is emitted by the source and passes through a pinhole aperture, which is located in front of the detector. The laser is reflected by a dichromatic mirror and scanned across the specimen.[32] The secondary fluorescence is emitted by the sample and passed through the dichromatic mirror and focused as a confocal

point at the detector pinhole aperture.[32] Figure 2.2 depicts this confocal light path. Compared to traditional widefield epi-fluorescence microscopy, confocal produces a much stronger signal.[32]

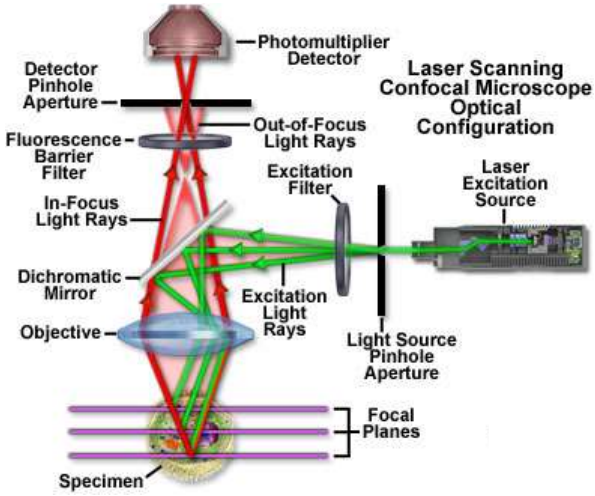

Figure 2.2 Confocal microscopy light pathway.[32]

Chapter 3

Methods

3.1 Material Manufacturing

Polyurethane Urea

Polyurethane urea samples were prepared at Hershey Medical Center using a modified protocol from Milner *et al*.[24] The PUU was created by successively spin casting and curing 18% Biospan MS/0.4 on a smooth PDMS mold three times. The first layer was spun at 1500 rpm for 60 seconds, which created a thin and smooth layer. The next layer was spun at 800 rpm for 60 seconds, and the final layer was spun at 400 rpm for 60 seconds. Following each casting, the sample cured overnight in a vacuum at room temperature. This process increased the thickness of the material, maintained smoothness, and reduced bubble formation. Figure 3.1 shows a PUU material sample prepared at Hershey Medical Center.

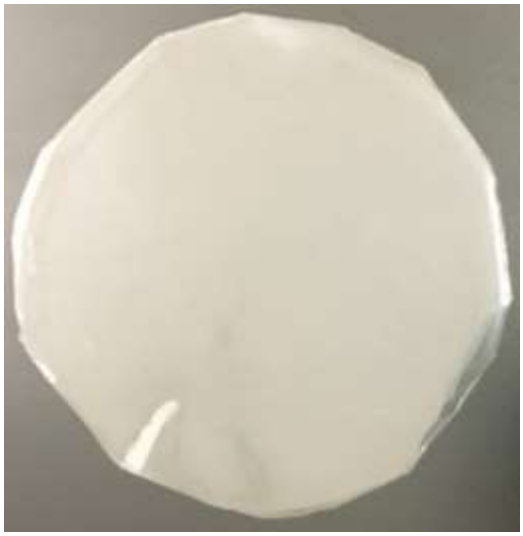

Figure 3.1 Polyurethane urea material sample prepared at Hershey Medical Center.

Polyetheretherketone

Two sets of polyetheretherketone samples were obtained. Three PEEK (machined, polished, and polished and machined) samples used for the x-ray photoelectron microscopy study were obtained from Hershey Medical Center. An example of one of the PEEK samples is seen in Figure 3.2. Polyetheretherketone samples used for the rotating disk system and optical profilometry studies were obtained from PEEK film created by Victrex APTIV (Dublin, Ireland) films. The films were manufactured to quality standards with high temperature performance, chemical resistance, high strength and toughness, and high purity with low extractables.[40] The PEEK material was tested with surface categorization techniques and cleaned prior to testing platelet adhesion. Figure 3.3 shows the raw PEEK film.

Figure 3.2 PEEK sample obtained from Hershey Medical Center.

Figure 3.3 Raw PEEK film purchased from Victrex APTIV.[40]

3.2 Material Preparation

Polyurethane Preparation

To prepare the material samples for the rotating disk system, a 20 mm diameter stamp was used to cut six circular pieces of the desired materials. The polyurethane samples were rinsed with deionized water and lightly dried to remove any impurities from the surface. The samples were placed into a beaker filled with deionized water 24 hours prior to experimentation for equilibration.

Polyetheretherketone Preparation

To prepare the material samples for the rotating disk system, a 20 mm diameter stamp was used to cut 12 circular pieces of the desired materials. The PEEK samples were placed into a beaker filled with deionized water 24 hours prior to experimentation for equilibration. For preparation of the "clean PEEK," six of the cut polyetheretherketone samples were cleaned by following an established cleaning protocol. The first stage of cleaning removed residue left from polishing that was visible to the naked eye. An additional two stages of cleaning ensured any remaining impurities from the polishing process were removed prior to analysis. The disks were inspected under the microscope to verify the effectiveness of the cleaning process.

3.3 Material Characterization Techniques

Material characteristics, in addition to platelet adhesion and hemocompatibility, are important aspects of biomaterial classification. Surface smoothness is a factor of consideration,

particularly for hemocompatibility within blood contacting surfaces.[19] In addition to surface topography and roughness, other surface properties such as surface free energy and wettability, surface chemistry and functional group contribute to the protein adsorption on the material surface as well as the blood-material interface.[18] The main surface characterization techniques used in the study were optical profilometry and x-ray photoelectron spectroscopy (XPS). Prior to analyzing platelet adhesion, the polyurethane and PEEK materials were studied using these techniques.

Optical Profilometry

Optical profilometry (Zygo Nextview 3D Optical Profilometer) was used to compare average surface roughness (Ra) and average surface irregularity (PV) from the respective manufacturing protocols of one sample of both biomaterials. Both the PEEK and polyurethane materials were analyzed with the optical profilometer. Figure 3.4 depicts the Zygo Nextview 3D Optical Profilometer.

Figure 3.4 Zygo Nextview 3D Optical Profilometer.[41]

X-Ray Photoelectron Spectroscopy

X-ray photoelectron spectroscopy (XPS) evaluation of the PEEK samples was used to determine any surface contamination resulting from the material manufacturing and polishing processes. Figure 3.5 shows the Physical Electronics VersaProbe II used to conduct XPS studies. This evaluation was performed by XPS experts in the Penn State Millennium Science Material Research Institute.

Figure 3.5 Physical Electronics VersaProbe II used for x-ray photoelectron spectroscopy studies.[42]

3.4 Blood Analysis Preparation

Bovine Plasma Preparation

Whole bovine blood was obtained from Penn State dairy barns. Bovine blood was drawn from the jugular vein of healthy bovines according an approved IACUC protocol. The whole blood was collected via a 16 G needle in a 500 mL donor bag containing citrate phosphate dextrose adenine-1 (CPDA-1) for anti-coagulation during the 20-minute transportation from the Penn State

dairy barn to the laboratory. Platelet viability and hemostatic effectiveness are maintained when stored at room temperature for short durations with CPDA-1.[26,27] Following transportation, the bovine blood was centrifuged at 600 G for 20 minutes at 25ºC with 1% acceleration and deceleration. The top layer of platelet rich plasma (PRP) was slowly and carefully removed using a 25 mL autopipette and placed into a separate 50 mL aliquot. During separation it was important to acquire as much PRP as possible without disturbing the buffy coat layer above the red blood cells (RBC). During separation, it was important to acquire as much PRP as possible without disturbing the buffy coat layer above the red blood cells. The remaining blood was centrifuged at 1500 G for 20 minutes to obtain platelet poor plasma (PPP). The top layer of PPP was removed and placed into a clean 50 mL aliquot. As with the PRP, it was important to remove the PPP without disturbing the red blood cells. The separation of the different layers of plasma from whole blood may be seen in Figure 3.6.

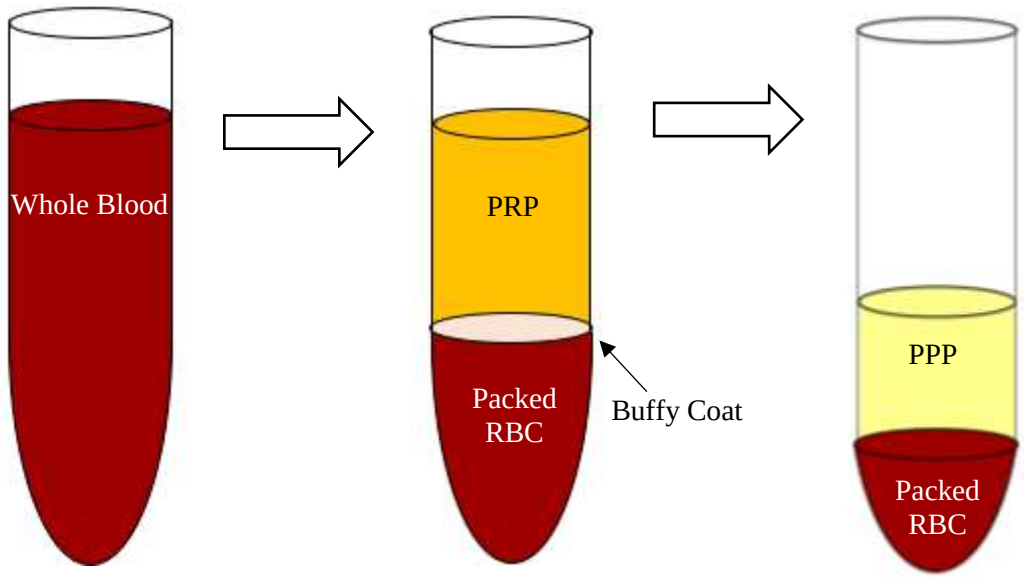

Figure 3.6 Process of centrifuging the whole blood into platelet rich plasma (PRP) and platelet poor plasma (PPP).

Standardized Platelet Concentrations

A hemocytometer (Hausser Scientific, Horsham, PA) and bright-field microscope (10x-40x magnification) was used to obtain platelet concentration measurements. The hemocytometer (Figure 3.7A) is an etched glass chamber with two plateaus with Neubauer rulings and two raised-edged moats that hold a cover-slip about 0.1 mm above the plateaus. The platelet rich plasma platelet concentration was calculated in platelets/mL by counting the total cell count in five squares of the same size (Figure 3.7B).

A **B**

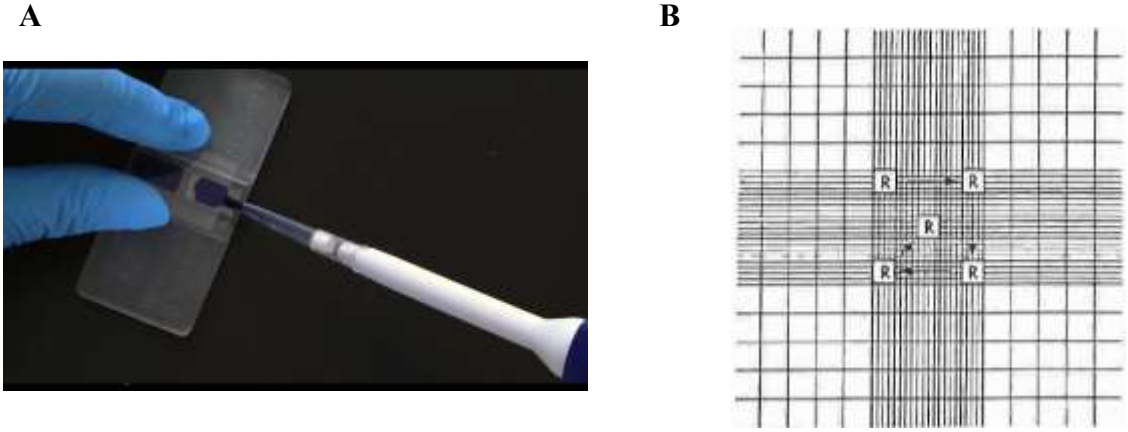

Figure 3.7 Platelet concentration quantified using (A) hemocytometer[28] within magnified (B) regions of interest.[29]

To achieve 50 mL of PRP at a bulk platelet concentration (C_∞) of 250 x 10^6 platelets/mL, Equation 2 and Equation 3 were used to determine the respective amounts of PRP and PPP.

$$\mathrm{Vol}_{prp} = \frac{50 \mathrm{x} 250}{\mathrm{PRPConc}} \quad [2]$$

$$\mathrm{Vol}_{ppp} = 50 - \mathrm{Vol}_{prp} \quad [3]$$

Density and Viscosity Measurements

Plasma density was calculated by weighing 1 mL of PRP. The average PRP viscosity was calculated at 30ºC over a range of shear rates using a viscoelastic analyzer (Vilastic Scientific, Austin, TX). Bovine plasma was calculated to have an average viscosity of 1.4553 cP. See Table A.1 in Appendix A for bovine viscosity data.

3.5 Disk Preparation

The stainless-steel metal disks used for the rotating disk system were 7.6 mm thick with inscribed concentric 1 mm circles with six 60º-spaced radial lines shown in Figure 3.8. The equilibrated PEEK or PUU material was removed from the deionized water and mounted to the 20 mm diameter metal disk with double-sided tape. The metal disk with the material was then equilibrated in phosphate buffered saline (PBS) (Sigma-Aldrich, St. Louis, MO) at 30ºC for 1 hour prior to rotation to allow the sample to reach the desired temperature. After 1 hour, the PBS was removed and replaced with the 50 mL of PRP in a 100 mL polytetrafluoroethylene (PTFE) beaker and maintained at 30ºC for the duration of the experiment (Figure 3.8).

3.6 The Rotating Disk System

The rotating disk system (RDS) is illustrated in Figure 3.8. The motor and shaft (Pine Instruments, Inc., Grove City, PA) attach to a steel thread adaptor that connects to the disk that holds the material. An adjustment knob on the front panel of the RDS motor controls the steady rotation speeds. The RDS motor maintained these speeds within 1% of the reading. Prior to

rotation, the disk was lowered approximately 3 mm into the PRP. The disk was steadily rotated at 283 rpm for 2 hours. As the disk rotates, the shear rate along the radial lines was able to be defined at the surface because velocity increases linearly with radial distance.

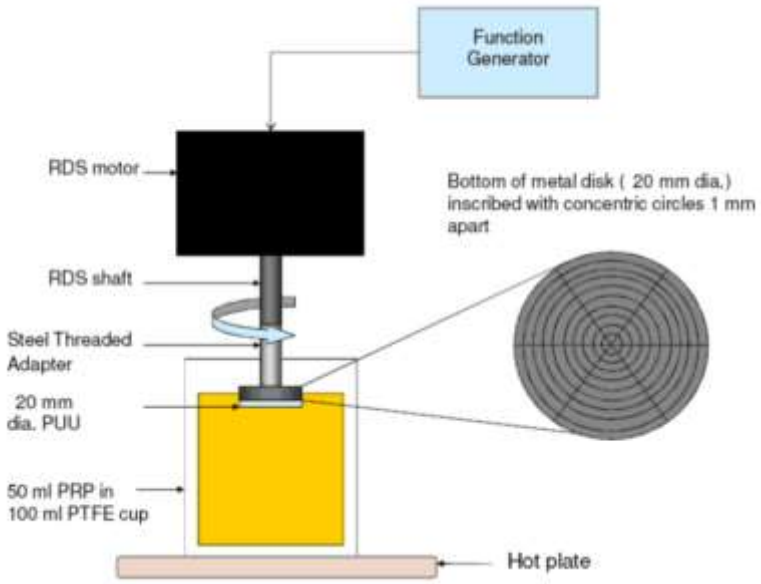

Figure 3.8 Rotating disk system used for platelet adhesion studies.[24]

Following the rotation, an autopipette was used to replace the PRP with 1x PBS by gently adding six 35 mL PBS additions while aspirating. Following the rinsing, the sample sat in the buffer solution for 10 minutes. The PBS was replaced with 1% paraformaldehyde (PFA) by gently adding six 35 mL PFA additions while aspirating. The sample fixed for an hour. The PFA was replaced with 1x PBS as described previously to rinse the disk between solutions for 10 minutes. At that point, the disk assembly was removed. The disk was then analyzed using one of two methods: scanning electron microscopy or confocal microscopy.

3.7 Imaging Techniques

Scanning Electron Microscopy Analysis

Scanning electron microscopy (SEM) imaging (Thermo Fisher (FEI) Q250) was used to validate the presence of platelets on the material surface and compare adherence of platelets on material surfaces. To prepare the samples for imaging, an ethanol dehydration protocol with solutions of increasing concentration from 30% to 100% was performed on the samples. The samples were then sputter coated in iridium to improve image contrast. SEM imagining was used to observe the platelets with 1000x and 3000x magnification.

Confocal Microscopy Analysis

For confocal microscopy analysis, the disk and adhered material were placed in a 12 well tray. The platelets adhered to the material surface were immunofluorescently labeled through treatment with a primary CAPP2A mouse anti-bovine $\alpha_{IIb}\beta_3$antibody (VMRD, Pullman, WA). This primary antibody solution was prepared by combining 2.25 µL CAPP2A and 1.5 mL 6% donkey serum (Sigma-Aldrich, St. Louis, MO)). The disk and material were required to be submerged in the solution throughout the incubation. The disk was incubated in the primary anti-body solution overnight at 4ºC in the refrigerator for complete binding between the primary antibody and the adhered platelets. The following day, the material surface was gently washed with five 3 mL PBS additions using a plastic pipette. A second pipette removed the non-specifically bound primary antibody while ensuring that the sample surface remained submerged. A secondary antibody solution was prepared by combining 1.5 mL of 6% donkey serum and 3.0 µL Alexa-Fluor 488

anti-mouse IgG (Invitrogen, Carlsbad, CA). The solution was added to the well containing the disk and material, and the disk was incubated at room temperature in the dark for 1 hour. The disk was again gently rinsed with PBS using the same procedure previously mentioned to remove non-specifically bound secondary antibody.

The disk was removed from the well and placed on a glass slide. Fifty microliters of an anti-fade solution (Biomeda Corp., Foster City, CA) was placed onto the material surface and a coverslip was applied carefully to avoid bubble formation between the sample and coverslip. The disk was kept in the refrigerator at 4ºC overnight to allow the gel to set.

The disk was imaged using a FV-1000 confocal microscope (Olympus Corporation, Shinjuku, Tokyo, Japan). The inscribed radial lines and concentric circles allowed for easy location identification. Furthermore, imaging at the intersections of the lines minimized bias in the data collection. A 10x objective (Olympus Corporation, Shinjuku, Tokyo, Japan) was used to locate the radial intersection of interest. A 20x dry objective (Olympus Corporation, Shinjuku, Tokyo, Japan) was used to image the sample. The numerical aperture (*NA*) of the lens is a dimensionless number used to characterize the range of light acceptance angles. The *NA* is calculated by Equation 4:

$$NA = n \sin \vartheta \qquad [4]$$

where n is the index of refraction of the medium and ϑ is the half-angle of the maximum cone of light that can enter the objective. The dry objective used air as a medium, and therefore has a value of n = 1.0. The image area produced by the scanning with the 20x objective was 530.33 μm^2 and centered on the particular radial intersection.

3.8 Platelet Adhesion Quantification

The platelet adhesion profile of each disk was quantified using an adhesion coefficient. The platelet counts at the nine radial intersections along two randomly chosen radial lines constituted one experiment. The adhesion coefficient is defined as the percentage of platelets that adhere to the material surface over the number of platelets that contact the surface due to disk rotation and particle diffusivity. This adhesion measurement was used by Wang *et al.* in 1993 and Milner *et al.* in 2006.[33, 24] Using platelet counts obtained from the confocal microscopy, the overall platelet adhesion for each of the PEEK and polyurethane samples was determined by calculating an adhesion coefficient (AC), which is defined as:

$$AC = \frac{N}{j*t} * 100 \quad [5]$$

where N is the average number of platelets per unit area, j is the mass flux, and t is the rotation time. The mass flux was defined as:

$$j = 0.62 D^{\frac{2}{3}} \nu^{-\frac{1}{6}} \omega^{\frac{1}{2}} C_{\infty} \quad [6]$$

where ω is the RMS angular velocity, C_{∞} is the bulk concentration, ν is the kinematic viscosity. The diffusivity (D) is defined as:

$$D = \frac{K_B T}{6\pi\eta b} \quad [7]$$

where K_B is the Boltzmann constant, T is the absolute temperature, η is the dynamic viscosity of PRP, and b is the average platelet radius.[33]

Chapter 4

Results

4.1 Material Characterization Results

Optical Profilometry

The optical profilometry results provided an analysis of the surface roughness of the PEEK and polyurethane materials. Measurements were obtained from 5 different surface locations on one sample of each material. The PEEK and polyurethane samples were both obtained from the same experimental materials used for platelet adhesion testing with RDS. The mean surface roughness (Ra) and largest surface irregularity measured from the centerline (PV) were measured from the entire surface of each sample. These results and standard deviations for each measurement are shown in Table 4.1. A sample PEEK surface (Figure 4.1A) with a surface roughness of 20 nm and a polyurethane surface (Figure 4.1B) with a surface roughness of 30 nm are shown. These samples most closely resembled the average surface roughness of each respective material.

Table 4.1 Optical profilometry average surface roughness (Ra) and average largest surface (PV) results from PEEK and polyurethane.

Sample	Average Ra [nm]	Ra SD [nm]	Average PV [nm]	PV SD [nm]
PEEK	20.2	3.6	989.8	772.3
Polyurethane	39.8	13.7	3136.4	1498.0

*

*Indicates statistically significant difference between the values. See Table A.5 in Appendix A.

A **B**

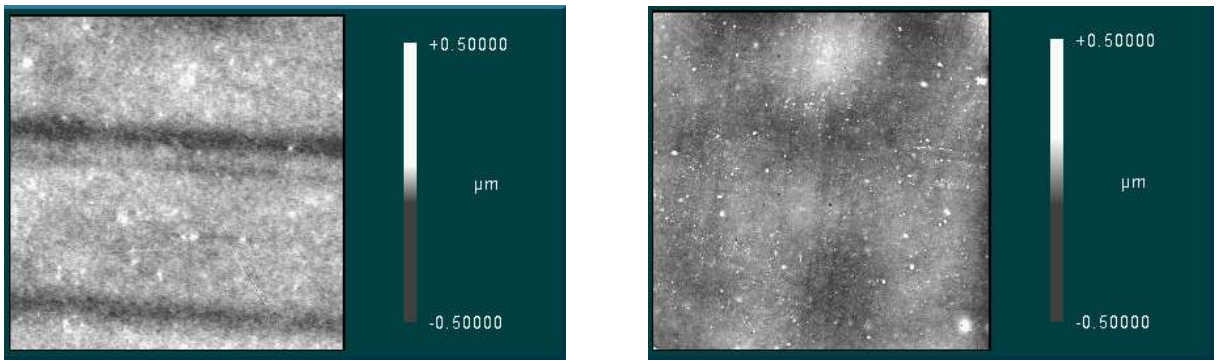

Figure 4.1 Sample optical profilometry results for (A) PEEK and (B) polyurethane. The color distribution represents the z-distance from the surface.

X-Ray Photoelectron Spectroscopy

The x-ray photoelectron spectroscopy studies (XPS) studies compared the machined PEEK, polished PEEK, and polished and washed PEEK samples from Hershey Medical Center. The measurements were made at a takeoff angle of 45º with respect to the surface plane of the sample. This measurement technique resulted in a typical sampling depth of 3-6 nm, which signified that 95% of the signal originated from this depth or shallower. Table 4.2 shows the

concentration of elements detected within the PEEK samples. These samples were compared to theoretical pure PEEK.

Table 4.2 XPS results for concentration of elements detected (in atom %) in the PEEK samples.

Sample	Carbon (%)	Oxygen (%)	Silicone (%)
Machined PEEK	87.4	12.5	0.1
Polished PEEK	79.3	16.1	4.5
Polished, Washed PEEK	86.7	13.1	0.2
PEEK Theory	86.4	13.6	-
PDMS Theory	50.0	25.0	25.0

The PEEK theory allowed for comparison of the various PEEK samples to an established criterion. The polydimethylsiloxane (PDMS) theory was used as a point of comparison to show any significant contamination from the polishing process.

4.2 Imaging Analysis Results

Scanning Electron Microscopy

Scanning electron microscopy (SEM) was used to validate the presence of platelets on the material surfaces and observe broad trends in platelet behavior. Figure 4.2 shows two sample

SEM images at 3000x magnification from polyurethane and PEEK samples. While using the SEM, the exact radial position on the disk was unable to be determined.

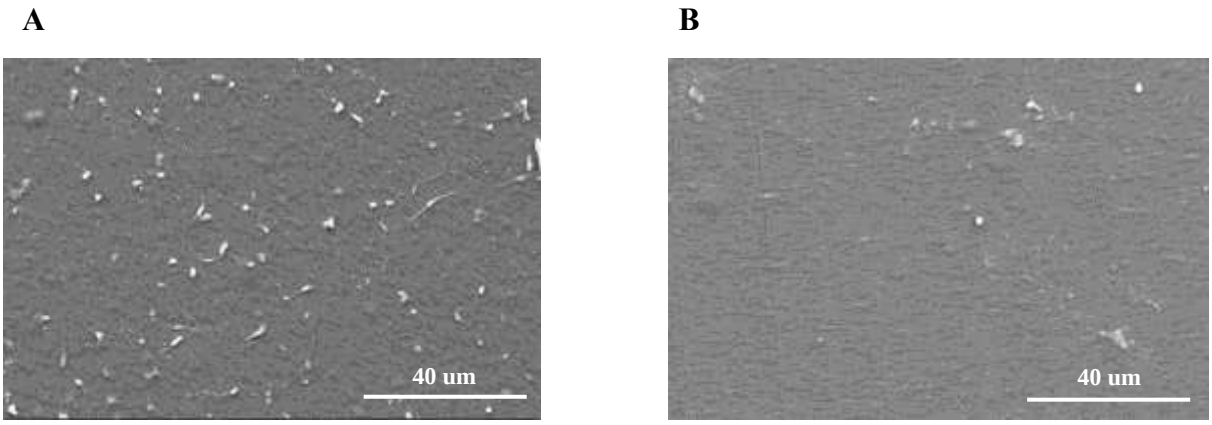

Figure 4.2 Scanning electron microscopy images with 3000x magnification from (A) polyurethane and (B) PEEK.

Confocal Microscopy

Confocal microscopy was the main imaging technique used to quantify the number of platelets located on each material surface. Three different materials were imaged: polyurethane, PEEK, and cleaned PEEK. The "cleaned" PEEK was classified as the PEEK material that had been cleaned using the cleaning protocol. A total of 18 images were obtained for each experimental disk with a dry 20x objective. Figures 4.3, 4.4, and 4.5 show sample confocal images from each of the materials. All images were from bovine-tested materials. Platelets adhered to the PEEK surfaces are circled in the images for clarification.

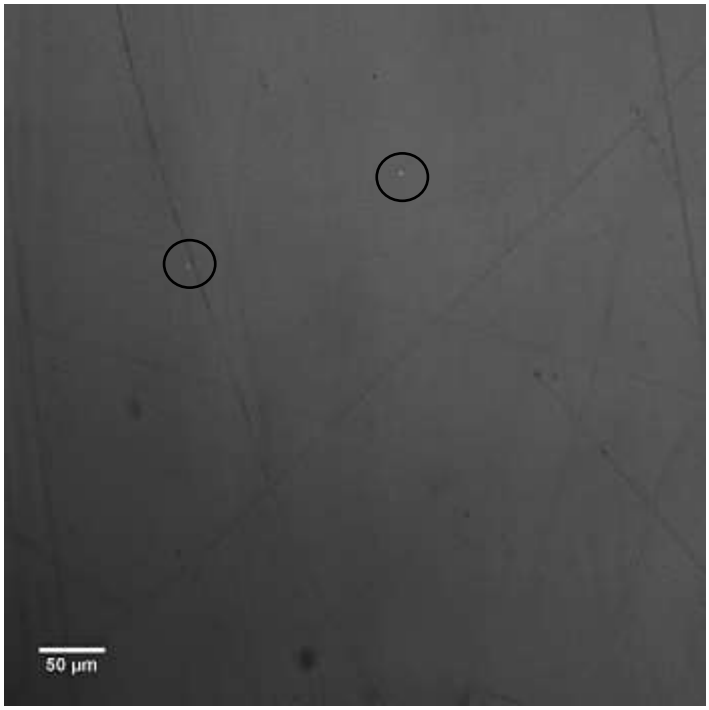

Figure 4.3 Confocal microscopy (20x) image of PEEK taken at a radial location of 3 mm.

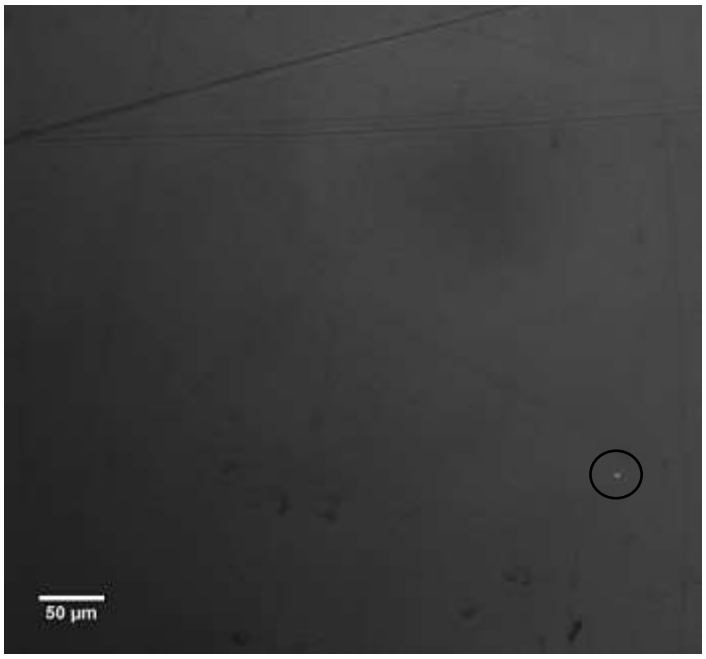

Figure 4.4 Confocal microscopy (20x) image of cleaned PEEK taken at a radial location of 3 mm.

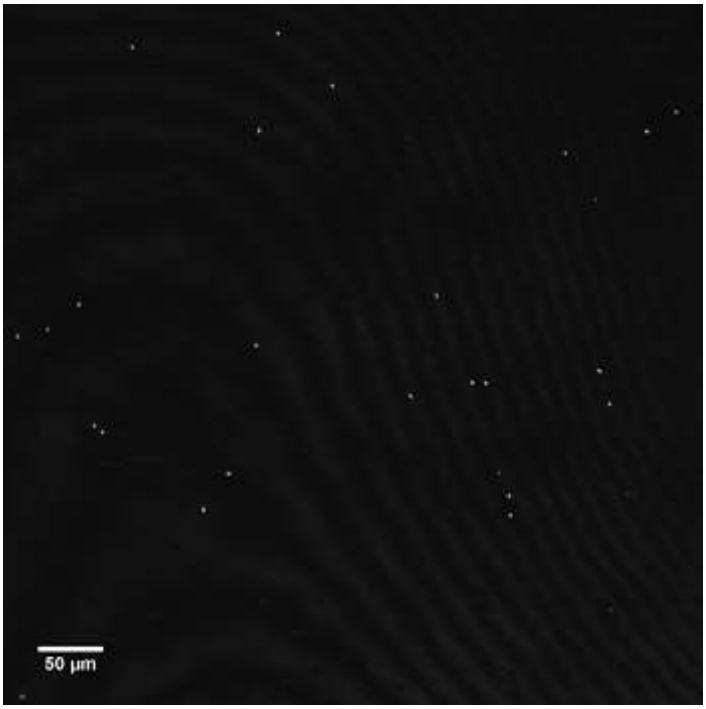

Figure 4.5 Confocal microscopy (20x) image of polyurethane taken at a radial location of 3 mm.

The images were obtained using similar confocal settings to maintain continuity across the material samples from each respective experiment. The platelet counts for each of the images were obtained by distinguishing individual regions within the images and counting each respective region and the fluorescing particles within those regions.

4.3 Platelet Adhesion Results

Bovine Platelet Adhesion

Using the average number of platelets per unit area from the confocal microscopy results, the mass flux, and the rotation time of the RDS protocol, the adhesion coefficients [5] were calculated for the PEEK, cleaned PEEK, and polyurethane samples for bovine plasma. Raw

platelet densities for these samples are found in Tables A.2, A.3, and A.4 in Appendix A. Error bars indicate the standard error of the mean at each corresponding shear rate. The three material adhesion results shown in Figure 4.6 directly compare the significance of peak shear exposure on the mean adhesion coefficient at each radial location. Significance is characterized by the Analysis of Variance Test (ANOVA) at a 95% confidence interval. The ANOVA test is a statistical method in which the variation in a set of groups or observations is divided into distinct components. Measurements were taken to compare the adhesion coefficients of three different materials at each respective shear rate. An post hoc test was performed to determine the significance between the PEEK and cleaned PEEK data. The results of these analyses are seen in Table A.6 in Appendix A.

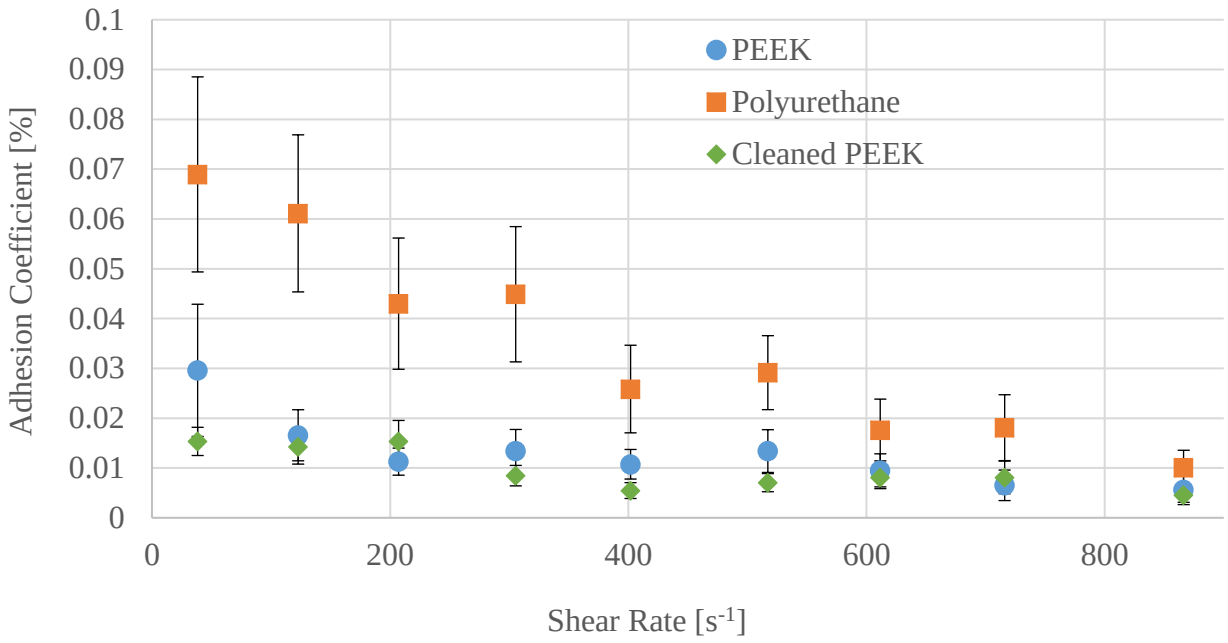

Figure 4.6 Bovine adhesion coefficient values vs. shear rate results for polyurethane, PEEK, and cleaned PEEK.

Chapter 5

Discussion

5.1 Discussion of Results

The results from the different analyses revealed certain correlating trends with the properties and adhesion behavior of the different biomaterials. Optical profilometry showed that the polyurethane surface was significantly rougher than the PEEK surface. The surface characteristics of the materials have a potential effect on the adhesion behavior of the polyurethane and PEEK materials. The differing values in the PEEK and polyurethane roughness values provide additional evidence for differences found in the platelet adhesion behavior on the material surfaces. Studies by Linneweber *et al.* analyzed the effect of surface roughness on the activation of the coagulation pathway and platelet adhesion in an impeller blood pump. The results showed that adhesion was 40 and 76% higher in surfaces differences.[43] These surface results indicate that minimal surface irregularities may contribute to altered adhesion behavior.

The XPS investigation confirmed that a post-processing cleaning protocol was able to successfully remove the PDMS and retain a pure PEEK surface chemistry. As seen in Table 4.2, the polished PEEK sample had a higher concentration of silicone (4.5%) compared to the minimal elemental concentration (0.1%) in the initial machined PEEK. The results showed that the elemental concentration of silicone was significantly decreased in the polished and washed sample. The polished and washed PEEK sample showed a strong correlation to the theoretical PEEK results with a percent error for the carbon concentration and oxygen concentration of 0.35% and 3.68%, respectively. These results were significant to the adjustment of the protocol to include the PEEK cleaning process. Furthermore, the results confirmed that the polished and

washed PEEK material is representative of the theoretical material properties. This verifies the necessity for the cleaning protocol and the significance of implementing it into the procedure. This investigation confirms that the cleaned PEEK used in the other protocols will be more representative of theoretical PEEK material.

The results from the scanning electron microscopy validated the observed trends in the confocal microscopy results. As seen in Figure 4.2, the presence of adhered platelets was confirmed through this study. The study also revealed a trend of decreasing platelet concentration as the radial distance from the center of the disk increased. Since the exact radial location on the disk could not be determined with the SEM imaging, no direct correlation between the positioning and the shear rate could be made. Lower platelet concentrations were found on the PEEK material compared to the polyurethane material. Both of the previously mentioned observations were replicated in the confocal microscopy studies.

The confocal microscopy results were validated by the material characterization and SEM studies. As seen in Figure 4.6, the adhesion coefficients decrease with increasing shear rate. The low adhesion for all three materials was observed beyond 400 s^{-1}. These observed trends are consistent with literature.[44,45] The results also showed higher adhesion rates in the polyurethane data compared to the PEEK, and similarly, higher adhesion in the PEEK compared to the cleaned PEEK material. The initial ANOVA statistical analysis showed that the adhesion coefficients at each respective shear rate of each material (PEEK, cleaned PEEK, and polyurethane) are statistically different as a group. A post-hoc Tukey HSD analysis showed that the differences between the PEEK and polyurethane and the cleaned PEEK are statistically different. However, the difference between the PEEK and cleaned PEEK is insignificant.

The adhesion coefficients allowed for a normalized platelet concentration across all materials and platelet species. The broad trends of lower platelet adhesion in the PEEK and clean PEEK and decreasing platelet adhesion with increasing radial distance were consistent throughout the study. These behaviors, which are consistent with previous studies, validate the findings within the bovine platelet and material interactions.[25,45] The results also show that there is overall minimal platelet adhesion in the PEEK data. Studies with PEEK and platelet adhesion have shown that the thrombogenicity of the surface of PEEK may be further reduced through PMPC graft layers.[58] The results from the adhesion coefficient data have been compared to previous studies from Navitsky *et al.*[25,45] This comparison of studies reveals similar trends in coefficient magnitude values at shear rates above 500 s^{-1}. This study, however, indicates very minimal adhesion overall, particularly in the PEEK materials, at any shear rate.

5.2 Future Research

The studies of the platelet behavior of different species was used to reflect past work and future animal trials that will be conducted with the Fontan blood pump. Future studies will quantify and explore the behavior of ovine platelets to PEEK and polyurethane materials. These studies will be used to compare the results from the bovine studies and further validate any findings in the platelet behavior with the PEEK and polyurethane materials. In order to introduce a well-documented control material to the study, OTS coated glass will be included into the bovine and ovine studies. These glass studies will create a standardized point of comparison for the adhesion results. Future studies will explore the adhesion behavior of human platelets so that the results are more applicable to human trials with the pump.

Appendix A

Table A.1 Viscosity data for bovine blood

Trial	Average Bovine Viscosity [cP]
1	1.4167
2	1.4940
Average	1.4553
Std.	0.054659

Table A.2 Raw platelet counts from polyurethane experiments.

Polyurethane Raw Platelet Counts												
Shear Rate	**Disk1 Line1**	**Disk1 Line2**	**Disk2 Line1**	**Disk2 Line2**	**Disk3 Line1**	**Disk3 Line2**	**Disk4 Line1**	**Disk 4 Line 2**	**Disk 5 Line 1**	**Disk 5 Line 2**	**Disk6 Line1**	**Disk6 Line2**
38.3723	29	14	14	7	139	61	6	7	30	12	36	30
122.745	40	16	15	60	67	35	13	7	13	15	16	13
207.117	26	33	14	18	23	40	5	16	8	15	55	6
305.489	42	26	8	11	23	39	9	10	23	8	36	32
401.862	9	15	9	6	19	33	6	5	8	14	40	9
517.234	19	12	8	6	21	36	3	3	12	8	16	2
611.607	15	13	6	8	5	15	1	8	4	10	26	11
715.979	20	11	2	8	7	10	4	5	4	11	27	21
866.351	10	11	1	4	6	4	1	1	10	8	9	4

Table A.3 Raw platelet counts from the PEEK experiments.

Polyetheretherketone Raw Platelet Counts												
Shear Rate	**Disk1 Line1**	**Disk1 Line2**	**Disk2 Line1**	**Disk2 Line2**	**Disk3 Line1**	**Disk3 Line2**	**Disk4 Line1**	**Disk 4 Line 2**	**Disk 5 Line 1**	**Disk 5 Line 2**	**Disk6 Line1**	**Disk6 Line2**
38.3723	10	12	4	62	62	6	3	2	0	3	4	0
122.745	8	4	3	28	24	3	2	3	6	2	3	8
207.117	12	6	2	8	15	7	4	0	2	1	6	1
305.489	11	3	0	5	27	5	1	1	8	2	3	10
401.862	6	0	2	9	17	0	5	3	8	0	2	9
517.234	5	5	1	9	23	0	1	3	19	5	1	4
611.607	4	0	2	9	20	1	1	1	6	0	3	7
715.979	0	0	0	2	19	1	1	2	1	4	2	5
866.351	0	0	0	0	18	0	2	0	5	4	2	1

Table A.4 Raw platelet counts from the cleaned PEEK experiments.

Cleaned Polyetheretherketone Raw Platelet Counts												
Shear Rate	**Disk1 Line1**	**Disk1 Line2**	**Disk2 Line1**	**Disk2 Line2**	**Disk3 Line1**	**Disk3 Line2**	**Disk4 Line1**	**Disk4 Line 2**	**Disk 5 Line 1**	**Disk 5 Line 2**	**Disk6 Line1**	**Disk6 Line2**
38.3723	8	9	6	8	11	6	4	3	0	17	2	13
122.745	2	6	1	1	15	3	12	2	8	15	6	15
207.117	3	2	2	3	20	0	5	5	12	16	1	18
305.489	1	3	3	0	9	5	2	4	1	9	1	10
401.862	1	1	0	2	3	2	8	2	8	3	1	1
517.234	1	7	0	1	10	3	7	2	4	3	15	1
611.607	2	5	3	0	4	2	14	3	8	2	3	3
715.979	2	10	5	0	1	2	19	2	5	0	12	0
866.351	1	8	0	0	1	1	6	3	1	0	2	3

Table A.5 ANOVA single factor analysis for optical profilometry roughness data.

SUMMARY

Groups	*Count*	*Sum*	*Average*	*Variance*
Column 1	5	4.949	0.9898	0.74563
Column 2	5	15.682	3.1364	2.805134

ANOVA

Source of Variation	*SS*	*df*	*MS*	*F*	*P-value*	*F crit*
Between Groups	11.51973	1	11.51973	6.488592	0.03432	5.317655
Within Groups	14.20306	8	1.775382			
Total	25.72278	9				

Table A.6 ANOVA single factor analysis for adhesion coefficient data.

SUMMARY

Groups	*Count*	*Sum*	*Average*	*Variance*
Column 1	9	0.116661	0.012962	5.06361E-05
Column 2	9	0.327954	0.036439	0.000332567
Column 3	9	0.086702	0.009634	1.77635E-05

ANOVA

Source of Variation	*SS*	*df*	*MS*	*F*	*P-value*	*F crit*
Between Groups	0.003842	2	0.001921	14.37421931	7.8708E-05	3.402826
Within Groups	0.003208	24	0.000134			
Total	0.00705	26				

BIBLIOGRAPHY

1. "Congenital Heart Defects." *Centers for Disease Control and Prevention*, www.cdc.gov/ncbddd/heartdefects/data.html#References.

2. "Critical Congenital Heart Disease." *U.S. National Library of Medicine*, National Institutes of Health, 18 Sept. 2018, ghr.nlm.nih.gov/condition/critical-congenital-heart-disease.

3. Hauck, Amanda, Nicolas Porta, Steve Lestrud, Stuart Berger. "The Pulmonary Circulation in the Single Ventricle Patient." *Children (Basel, Switzerland)*, vol. 4, no. 8, Multidisciplinary Digital Publishing Institute (MDPI), Aug. 2017, doi:10.3390/children4080071.

4. F. Fontan and E. Baudet, "Surgical repair of tricuspid atresia.," Thorax, vol. 26, no. 3, pp. 240–8, May 1971.

5. Fredenburg, Tyler B., et al. "The Fontan Procedure: Anatomy, Complications, and Manifestations of Failure." *RadioGraphics*, vol. 31, no. 2, Radiological Society of North America, Mar. 2011, pp. 453–63, doi:10.1148/rg.312105027.

6. Gewillig, Marc. "The Fontan Circulation." *Heart (British Cardiac Society)*, vol. 91, no. 6, BMJ Publishing Group, June 2005, pp. 839–46, doi:10.1136/hrt.2004.051789.

7. *STS Congenital Heart Surgery Database*. https://www.sts.org/registries-research-center/sts-national-database/sts-congenital-heart-surgery-database. Accessed 21 Sept. 2018.

8. De Rita, Fabrizio, D. Crossland, M. Griselli, A. Hasan. "Management of the Failing Fontan." *Seminars in Thoracic and Cardiovascular Surgery: Pediatric Cardiac Surgery Annual*, vol. 18, no. 1, W.B. Saunders, Jan. 2015, pp. 2–6, doi:10.1053/J.PCSU.2015.01.004.

9. Khairy, Paul, S.M. Fernandes, J.E. Mayer, J.K. Triedman, E.P. Walsh. *Long-Term Survival, Modes of Death, and Predictors of Mortality in Patients With Fontan Surgery*. 2008,

doi:10.1161/CIRCULATIONAHA.107.738559.

10. Giridharan, G.A., M. Ising, M.A. Sobieski, S.C. Koenig, J. Chen, S. Frankel, M.D. Rodefeld. "Cavopulmonary assist for the failing Fontan circulation: impact of ventricular function on mechanical support strategy.," *ASAIO J.*, vol. 60, no. 6, pp. 707–15, 2014.
11. Weinstein, Samuel, R. Bello, C. Pizzaro, F. Flynn-Thompson, J. Kirklin, K. Guleserian, R. Woods, C. Tjossem, R. Kroslowitz, P. Friedmannm R. Jaquiss. "The Use of the Berlin Heart EXCOR in Patients with Functional Single Ventricle." *The Journal of Thoracic and Cardiovascular Surgery*, vol. 147, 2014, pp. 697–705, doi:10.1016/j.jtcvs.2013.10.030.
12. "An Overview of PEEK Biomaterials." *PEEK Biomaterials Handbook*, William Andrew Publishing, Jan. 2012, pp. 1–7, doi:10.1016/B978-1-4377-4463-7.10001-6.
13. Marois, Yves, and Robert Guidoin. *Biocompatibility of Polyurethanes*. Landes Bioscience, 2013, https://www.ncbi.nlm.nih.gov/books/NBK6422/.
14. "PEEK." Polyfluor, www.polyfluor.nl/en/materials/peek/.
15. Yan, Y., et al. "Contact Activation by the Intrinsic Pathway of Blood Plasma Coagulation." *Hemocompatibility of Biomaterials for Clinical Applications*, Woodhead Publishing, Jan. 2018, pp. 3–28, doi:10.1016/B978-0-08-100497-5.00001-X.
16. "Platelet Count ." Lab Tests Online, labtestsonline.org/tests/platelet-count.
17. Ruggeri, Zaverio M. "Platelet Adhesion under Flow." *Microcirculation (New York, N.Y. : 1994)*, vol. 16, no. 1, NIH Public Access, Jan. 2009, pp. 58–83, doi:10.1080/10739680802651477.
18. Xu, Li-Chong, J. W. Bauer, C.A. Siedlecki. "Proteins, Platelets, and Blood Coagulation at Biomaterial Interfaces." *Colloids and Surfaces. B, Biointerfaces*, vol. 124, NIH Public Access, Dec. 2014, pp. 49–68, doi:10.1016/j.colsurfb.2014.09.040.

19. Weiss, Douglas J. *COMPARATIVE PHYSIOLOGY OF PLATELETS FROM DIFFERENT SPECIES 17.1 INTRODUCTION*. 1999, https://link.springer.com/content/pdf/10.1007%2F978-1-4615-5049-5_17.pdf.

20. Goodman, S. L. "Sheep, Pig, and Human Platelet-Material Interactions with Model Cardiovascular Biomaterials." *Journal of Biomedical Materials Research*, vol. 45, no. 3, June 1999, pp. 240–50, http://www.ncbi.nlm.nih.gov/pubmed/10397982.

21. J. A. Hubbell and L. V. McIntire, "Visualization and analysis of mural thrombogenesis on collagen, polyurethane and nylon," Biomaterials, vol. 7, no. 5, pp. 354–363, Sep. 1986.

22. V. Balasubramanian and S. M. Slack, "The effect of fluid shear and co-adsorbed proteins on the stability of immobilized fibrinogen and subsequent platelet interactions.," J. Biomater. Sci. Polym. Ed., vol. 13, no. 5, pp. 543–61, 2002.

23. Schwiderski, Ernst W., and Hans J. Lugt. *Rotating Flows Over a Rotating Disk*. 1964, http://www.dtic.mil/dtic/tr/fulltext/u2/601195.pdf.

24. Milner, Keith R., A.J. Snyder, C.A. Siedlecki. "Sub-Micron Texturing for Reducing Platelet Adhesion to Polyurethane Biomaterials." *Journal of Biomedical Materials Research Part A*, vol. 76A, no. 3, Mar. 2006, pp. 561–70, doi:10.1002/jbm.a.30554.

25. Navitsky, Michael A., Steven Deutsch, Keefe B. Manning. "A Thrombus Susceptibility Comparison of Two Pulsatile Penn State 50 Cc Left Ventricular Assist Device Designs." *Annals of Biomedical Engineering*, vol. 41, no. 1, NIH Public Access, Jan. 2013, pp. 4–16, doi:10.1007/s10439-012-0627-z.

26. R. A. Kahn, S. D. Staggs, W. V Miller, and W. A. Heaton, "Recovery, lifespan, and function of CPD-Adenine (CPDA-1) platelet concentrates stored for up to 72 hours at 4 C.," *Transfusion*, vol. 20, no. 5, pp. 498–503.

27. E. P. Scott and S. J. Slichter, “Viability and function of platelet concentrates stored in CPD-adenine (CPDA-1).,” *Transfusion*, vol. 20, no. 5, pp. 489–97.

28. “Counting Cells with a Hemocytometer.” [Online]. Available: https://www.youtube.com/watch?v=pP0xERLUhyc. [Accessed: 26-Dec-2018].

29. P. J. Hansen, “Use of a Hemacytometer.”

30. J. W. Daily and R. E. Nece, “Chamber Dimension Effects on Induced Flow and Frictional Resistance of Enclosed Rotating Disks,” *J. Basic Eng.*, vol. 82, no. 1, p. 217, Mar. 1960.

31. E. R. Benton, “On the flow due to a rotating disk,” *J. Fluid Mech.*, vol. 24, no. 04, p. 781, Apr. 1966.

32. T. J. Fellers and M. W. Davidson, “Introduction to Confocal Microscopy.” [Online]. Available: http://olympus.magnet.fsu.edu/primer/techniques/confocal/confocalintro.html. [Accessed: 26-Dec-2018].

33. I. W. Wang, J. M. Anderson, and R. E. Marchant, “Staphylococcus epidermidis adhesion to hydrophobic biomedical polymer is mediated by platelets.,” *J. Infect. Dis.*, vol. 167, no. 2, pp. 329–36, Feb. 1993.

34. S. Nayak and P. D. Booker, “The Fontan circulation,” *Contin. Educ. Anaesth. Crit. Care Pain*, vol. 8, no. 1, pp. 26–30, Feb. 2008.

35. A. Pelagalli *et al.*, “Adhesive Properties of Platelets from Different Animal Species,” *J. Comp. Pathol.*, vol. 128, no. 2–3, pp. 127–131, Feb. 2003.

36. X. Wei *et al.*, “Mechanical Circulatory Support of a Univentricular Fontan Circulation with a Continuous Axial-Flow Pump in a Piglet Model,” *ASAIO J.*, vol. 61, no. 2, pp. 196–201, 2015.

37. K. Heidman, “NASA Glenn Technology Pumps Hope into Broken Hearts,” 2016.

38. A. L. Throckmorton, K. K. Ballman, C. D. Myers, S. H. Frankel, J. W. Brown, and M. D. Rodefeld, “Performance of a 3-Bladed Propeller Pump to Provide Cavopulmonary Assist in the Failing Fontan Circulation,” *Ann. Thorac. Surg.*, vol. 86, no. 4, pp. 1343–1347, Oct. 2008.

39. J. Cysyk., J.B. Clark, R. Newswanger, C.S. Jhun, J. Izer, H. Finicle, J. Reibson, B. Doxtater, W. Weiss, G. Rosenberg, “Chronic In Vivo Test of a Right Heart Replacement Blood Pump for Failed Fontan Circulation.,” *ASAIO J.*, Oct. 2018.

40. “High Performance Film for Unmatched Versatility and Performance.”

41. M. Fedkin and J. A. Dutton, “Optical Profilometer Training.” [Online]. Available: https://www.e-education.psu.edu/mcl-optpro/. [Accessed: 5-Mar-2019].

42. “X-Ray Photoelectron Spectroscopy (XPS).” [Online]. Available: https://www.mri.psu.edu/materials-characterization-lab/characterization-techniques/x-ray-photoelectron-spectroscopy-xpsesca. [Accessed: 5-Mar-2019].

43. J. Linneweber, P. M. Dohmen, U. Kerzscher, K. Affeld, Y. Nosé, and W. Konertz, “The Effect of Surface Roughness on Activation of the Coagulation System and Platelet Adhesion in Rotary Blood Pumps,” *Artif. Organs*, vol. 31, no. 5, pp. 345–351, May 2007.

44. Bluestein D, W. Yin, K. Affeld, J. Jesty. “Flow-induced platelet activation in mechanical heart valves.” *J. Heart Valve Dis.* Vol. 13, pp. 501–508, 2004.

45. M. A. Navitsky, J.O. Taylor, A.B. Smith, M.J. Slattery, S. Deutsch, C.A. Siedlecki, K.B. Manning, “Platelet adhesion to polyurethane urea under pulsatile flow conditions.,” *Artif. Organs*, vol. 38, no. 12, pp. 1046–53, Dec. 2014.

46. D. Mozaffarian *et al.*, “Heart Disease and Stroke Statistics—2015 Update,” *Circulation*, vol. 131, no. 4, Jan. 2015.

47. A. L. Throckmorton, K. K. Ballman, C. D. Myers, K. N. Litwak, S. H. Frankel, and M. D. Rodefeld, “Mechanical Cavopulmonary Assist for the Univentricular Fontan Circulation Using a Novel Folding Propeller Blood Pump,” *ASAIO J.*, vol. 53, no. 6, pp. 734–741, Nov. 2007.

48. A. L. Throckmorton and R. A. Kishore, “Design of a Protective Cage for an Intravascular Axial Flow Blood Pump to Mechanically Assist the Failing Fontan,” *Artif. Organs*, vol. 33, no. 8, pp. 611–621, Aug. 2009.

49. A. L. Throckmorton, Jugal Y. Kapadia, Steven G. Chopski, Sonya S. Bhavsar, William B. Moskowitz, Scott D. Gullquist, James J. Gangemi, Christopher M. Haggerty, Ajit P. Yoganathan, “Numerical, Hydraulic, and Hemolytic Evaluation of an Intravascular Axial Flow Blood Pump to Mechanically Support Fontan Patients,” *Ann. Biomed. Eng.*, vol. 39, no. 1, pp. 324–336, Jan. 2011.

50. “Platelets.” [Online]. Available: https://www.britannica.com/science/blood-biochemistry/Platelets-thrombocytes. [Accessed: 25-Mar-2019].

51. R. I. Litvinov and J. W. Weisel, “What Is the Biological and Clinical Relevance of Fibrin?,” *Semin. Thromb. Hemost.*, vol. 42, no. 4, pp. 333–43, Jun. 2016.

52. “Fibrin.” [Online]. Available: https://www.britannica.com/science/fibrin. [Accessed: 25-Mar-2019].

53. J. L. Gair *et al.*, “Strong process-structure interaction in stoveable poly(urethane-urea) aligned carbon nanotube nanocomposites,” *Compos. Sci. Technol.*, vol. 166, pp. 115–124, Sep. 2018.

54. “Properties of Polyetherketones.” [Online]. Available: http://polymerdatabase.com/polymer classes/Polyetherketone type.html. [Accessed: 25-Mar-2019].

55. M. Sharma, H. Sharma, and S. Shannigrahi, “Tribology of advanced composites/biocomposites materials,” *Biomed. Compos.*, pp. 413–429, Jan. 2017.

56. “Element and Processing,” *Interface Sci. Technol.*, vol. 18, pp. 431–499, Jan. 2011.

57. “Scanning Electron Microscopy (SEM).” [Online]. Available: https://serc.carleton.edu/research_education/geochemsheets/techniques/SEM.html. [Accessed: 25-Mar-2019].

58. Tateishi, Takaharu, Masayuki Kyomoto, Sachiro Kakinoki, Tetsuji Yamaoka, Kazuhiko Ishihara. "Reduced platelets and bacteria adhesion on poly (ether ether ketone) by photoinduced and self-initiated graft polymerization of 2-methacryloyloxyethyl phosphorylcholine." *Journal of Biomedical Materials Research Part A*, vol 102.5, pp. 1342-1349, 2014.

ACADEMIC VITA of CLARE MCHUGH

EDUCATION

THE PENNSYLVANIA STATE UNIVERSITY, UNIVERSITY PARK, PA Sept. 2015 – May 2019
COLLEGE OF ENGINEERING | SCHREYER HONORS COLLEGE
Bachelor of Science in Biomedical Engineering | Bachelor of Science in Mechanical Engineering

HONORS & AWARDS: Dean's List (All Semesters), Academic Excellence Scholarship (Fall 2015), President's Award (Fall 2015), Gatehouse Scholarship (Fall 2016), Kenneth Graham Excellence Scholarship (Spring 2017), Student Engagement Network Grant (Summer 2018), Schreyer Honors College Grant (Summer 2018), Distinguished Alumni Mentoring Program Protégé (Fall 2018-Spring 2019)

TECHNICAL SKILLS: 3Matic, Comsol, MATLAB, Microsoft Office, Mimic, R, SolidWorks

WORK EXPERIENCE

ARTIFICIAL HEART AND CARDIOVASCULAR FLUID DYNAMICS LAB STATE COLLEGE, PA
Research Assistant April 2017 – Present

- Developing an implantable pump for long-term, sustained mechanical support of patients with a failing Fontan circulation
- Working throughout the study in collaboration with medical professionals at Penn State Hershey Medical Center
- Perform analysis of blood-contacting poly-ether-ether-ketone (PEEK) material and categorizing its thrombosis potential

NSF INTERNATIONAL, HEALTH SCIENCES- MEDICAL DEVICES WASHINGTON, D.C.
Regulatory Research Intern May 2017 – Aug. 2017

- Researched and designed medical device regulatory content for international countries involved in MDSAP Audit Program
- Assessed the information and assisted in developing learning modules for clients within the medical device industry
- Trained in Regulation (EU) 2017/745 (Medical Device Regulation) and the Medical Device Single Audit Program (MDSAP)
- Certified ISO 13485:2016 Lead Auditor

ESSENTIAL MEDICAL INC. MALVERN, PA
Research and Development Intern May 2016 – Aug. 2016

- Completed data analyses, procedural reports, testing, and evaluations on large bore closure devices
- Assisted in the developmental testing and construction of an updated version of the device
- Manufactured and inspected devices for specified requirements within a sterile cleanroom environment
- Performed deployments of the device within a physiological model meant to simulate in-vivo conditions

PENN STATE COLLEGE OF ENGINEERING UNIVERSITY PARK, PA
Career Envoy Sept. 2016 – Present

- Peer mentor for students in the College of Engineering to assist fellow engineering students with professional development
- Hold weekly office hours and schedule individual appointments to review and improve resumes and cover letters
- Coordinate classroom presentations on topics ranging from interviewing to proper etiquette in a professional setting